

# Analysis of SDSS J125949.16+363036.3, a potential Hypervelocity Star

Andreas Finkler

12.10.2012

Friedrich-Alexander-Universität Erlangen-Nürnberg

supervised by Prof. Dr. Ulrich Heber and Eva Ziegerer

Hypervelocity Stars are fast enough to overcome the force of the Galactic potential and have unbound trajectories.

SDSS J090744.99+024506.8, also known as “The Outcast Star”, was found in 2005 by Brown, confirming the existence of HVS which were theoretically predicted in the late 1980s. Such extraordinary fast stars are most likely produced in what is called the slingshot mechanism. A binary system getting very close to the supermassive black hole at the Galactic center is torn apart. One of the stars is being captured by the black hole, whereas the other is ejected with a velocity of the order of 1000km/s. However, the Galactic halo hosts other classes of old stars that move almost as fast as the local escape velocity. Distinguishing Hypervelocity stars from extreme halo stars requires careful analysis.

The aim of this project is to investigate SDSS J125949+363036, a star with an unusually high proper motion. With the available SDSS spectra its distance, velocity, age and origin shall be determined.



**FRIEDRICH-ALEXANDER  
UNIVERSITÄT  
ERLANGEN-NÜRNBERG**

# Contents

<b>1</b>	<b>Introduction</b>	<b>3</b>
<b>2</b>	<b>Astrophysical Background</b>	<b>3</b>
2.1	Basic quantities . . . . .	3
2.1.1	Energy flux, flux density and luminosity . . . . .	3
2.1.2	Magnitudes and colors . . . . .	4
2.1.3	Effective temperature . . . . .	4
2.1.4	Metallicity . . . . .	5
2.2	Coordinate systems . . . . .	5
2.2.1	The equatorial coordinate system . . . . .	5
2.2.2	The galactic coordinate system . . . . .	6
2.2.3	The Galactic rest frame . . . . .	6
2.3	Structure of the Milky Way . . . . .	7
2.3.1	The Galactic potential . . . . .	7
2.4	Stellar evolution . . . . .	9
<b>3</b>	<b>Quantitative Spectroscopy</b>	<b>10</b>
3.1	Model atmospheres . . . . .	10
3.2	Deriving atmospheric parameters . . . . .	11
<b>4</b>	<b>Kinematics</b>	<b>12</b>
4.1	Distance determination . . . . .	12
4.2	Proper motion . . . . .	14
<b>5</b>	<b>Analysis of J125949.16+363036.3</b>	<b>15</b>
5.1	Modeling the atmosphere . . . . .	15
5.2	Mass and age determination . . . . .	18
5.3	A few words on error estimation . . . . .	20
5.4	Distance and velocity . . . . .	20
5.5	Examination of J1259+3630's possible origin . . . . .	21
<b>6</b>	<b>Summary and Outlook</b>	<b>31</b>
	<b>References</b>	<b>34</b>

# 1 Introduction

The Sun orbits the Galactic center at a rotational velocity of about 220km/s. This velocity lies well below the amount that is needed to overcome the gravitational pull that keeps it bound to the Milky Way. There is no chance the Sun gets to see what is outside of our galaxy, it is born in it and it will die in it. This is the fate for almost all stars in our galaxy. But in the year 1988 Hills [9] showed with numerical simulations that an interaction of a binary system with a massive black hole could lead to stars with velocities up to 4000km/s. With the galactic escape velocity lying at around 450km/s this is far enough for a star to travel beyond the boundaries of the Milky Way. Hills theory, nowadays known as the Hills or slingshot mechanism, states that a system of two or more stars making close encounter with a massive black hole can get torn apart. The black hole captures one of the companions and recoils the other. Even though two more production mechanisms with similar ejection velocities were suggested by Yu and Tremaine [28], the Hills mechanism remains the most likely one. Yu and Tremaine additionally introduced the idea of an encounter of two single stars and an encounter of a single star with a binary black hole. In 2005, Brown found a star that, due to its velocity, could indeed be explained with Hill's theory [4]. He discovered SDSS J090745.0+024507 which is speeding away from the Galactic center with a radial velocity of over 700km/s. In the same year, two Hypervelocity Stars were found by Hirsch et al. [10] and Edelmann et al. [7]. At the present day, only 22 unbound Hypervelocity Stars are known. This is not very astonishing since the production rates for the Hills mechanism predict only one to tenthousand Hypervelocity Stars in our Milky Way. With a total population of approximately 100 billion stars those extraordinary fast ones are very scarce.

In this work, the possible HVS candidate SDSS J125949.16+363036.3 is studied in order to gain knowledge of its Galactic rest frame velocity and possible origin. The star was selected because of its unusually high proper motion. Spectra and magnitudes are taken from the *Sloan Digital Sky Survey* (SDSS) Data Release 9.

## 2 Astrophysical Background

### 2.1 Basic quantities

In this Section the quantities used in this work are explained and their definitions given.

#### 2.1.1 Energy flux, flux density and luminosity

The major part of information obtained in this work is based on the star's optical spectrum. Here the energy flux is plotted against the wavelength. Hence a proper definition of what flux means is necessary. There are two kinds of fluxes that need to be distinguished: the *radiative flux*  $F_\nu$  that is given at a certain frequency  $\nu$  and the total *flux* which is the radiative flux integrated over all frequencies. The definition of the flux is given as the rate of energy transfer per unit area and is therefore given in units of  $\text{Wm}^{-2}\text{s}$  (for the radiative flux at a certain wavelength) or  $\text{Wm}^{-2}$  (for the total flux).

The luminosity of a star is linked to the flux. It is defined as the energy radiated by a star per unit time and can be expressed as

$$L = \oint_{\text{Sphere}} f dS = 4\pi d^2 f \quad (2.1)$$

Thus calculating a star's luminosity requires knowledge of its distance.

### 2.1.2 Magnitudes and colors

Magnitudes measure the brightness of a star. The classification of stars according to their apparent brightness goes back to the second century B.C., when it was of course not known that the human eye does not correspond linearly to the brightness of the incoming light. Magnitudes are therefore logarithmic quantities. Different magnitude systems exist. Without knowing an objects' distance, all we can say is based on the flux that is measured on Earth. For example, the apparent magnitude is defined as

$$m = -2.5 \log \left( \frac{f}{f_0} \right) \quad (2.2)$$

where  $f$  donates the total flux density and  $f_0$  refers to the historically set zero point of the magnitude. What we will need later on for our calculations is the *visual magnitude*  $m_V$  which instead of  $f$  uses the flux integrated over the visual band. But if we want to compare the brightness of two stars, we need the *absolute magnitude*  $M$  which involves the stars distance by using the star's luminosity:

$$M = -2.5 \log \left( \frac{L}{L_0} \right) \quad (2.3)$$

Precise measurements of magnitudes are made by using photoelectric photometers equipped with filters that only allow certain wavelength bands to pass. In our case the SDSS uses ugriz-filters corresponding to ultraviolet, green, red and two wavelength regions of infrared.

### 2.1.3 Effective temperature

One can not simply assign a single temperature to a star since it varies within the different regions. Instead the *effective temperature*  $T_{\text{eff}}$  is defined as the temperature at which the total flux emitted by a black body equals the total flux at the star's surface. This can be expressed with the Stefan-Boltzmann law

$$F = \sigma T_{\text{eff}}^4 \quad (2.4)$$

with the Stefan-Boltzmann constant  $\sigma$ .

### 2.1.4 Metallicity

The chemical composition of a star can again be characterized by several quantities. We use the *metallicity* which is defined as the logarithm of the ratio of iron abundance to hydrogen abundance compared to that of the Sun:

$$[Fe/H] = \log \left( \frac{N_{Fe}}{N_H} \right) - \log \left( \frac{N_{Fe}}{N_H} \right)_{\odot} \quad (2.5)$$

Thus the chemical composition of a star with  $[Fe/H] = 0$  equals the composition of the Sun.

Sometimes the metal mass fraction  $Z$  is used instead of the metallicity.

## 2.2 Coordinate systems

In the course of this work we will make use of different coordinate systems. This section explains the ones used.

### 2.2.1 The equatorial coordinate system

The equatorial coordinate system is geocentric, i.e. a coordinate system with the center of the Earth at its origin. It is commonly used to identify objects on the celestial sphere and consists of the two coordinates right ascension  $\alpha$  and declination  $\delta$ . One of the main advantages over other geocentric coordinate systems such as the horizontal coordinate system is that the equatorial coordinate system is independent of the observer's position. The projection of the Earth's equator onto the celestial sphere is called the celestial equator. Perpendicular to the plane of the celestial equator are the North celestial pole and the South celestial pole. A celestial meridian, also called an hour circle, connects the two poles with a great circle on the celestial sphere. In order to derive a coordinate system that is independent of the Earth's rotation, one has to determine a primary direction. Defining the ecliptic as the intersection of the Earth's orbital plane with the celestial sphere, one gets two points where celestial equator and ecliptic intersect. These are called vernal and autumnal equinox. The primary direction is given by the direction from the center of the Earth towards the vernal equinox. Figure 2.1 illustrates the equatorial coordinate system.

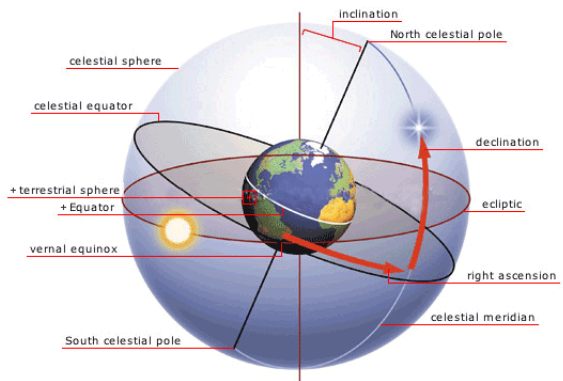


Figure 2.1: Equatorial coordinate system

Both declination and right ascension are angular distances. Declination gives the angular distance perpendicular to the celestial equator. By definition it is positive to the

north and negative to the south with the zero-point at the equator. Right ascension measures the angular distance from the vernal equinox eastward along the celestial equator to the hour angle. In general it is given in sidereal hours, minutes and seconds rather than in degrees.

Note that due to the precession and nutation of the Earth's axis the coordinate system is slowly rotating in time. Thus it is necessary to know the epoch in which the coordinates are given. An epoch defines the vernal equinox of a specific date.

### 2.2.2 The galactic coordinate system

In contrast to the equatorial coordinate system, the galactic coordinate system has the Sun at its origin. The primary direction is now given as the direction from the Sun towards the approximate center of the Milky Way and the fundamental plane lies in the assumed galactic plane. Instead of declination and right ascension the coordinates are now given as longitude  $l$  and latitude  $b$  (see Figure 2.2).

Measured eastward, the longitude  $l$  defines the angular distance on the galactic equator from the Galactic center. The latitude  $b$  measures the angular distance perpendicular to the galactic plane, positive to the north galactic pole and negative to the south galactic pole.

Other than the equatorial coordinate system, the galactic latitude and longitude are usually given in degrees.

### 2.2.3 The Galactic rest frame

With the Galactic rest frame, we finally arrive at a coordinate system that is independent of the Sun's orbital motion. It is a simple cartesian coordinate system with the Galactic center at the origin. The axes are labelled X, Y and Z with the X axis directed from the Sun towards the Galactic center with increasing values. Perpendicular to the X axis in the galactic plane lies the Y axis. Finally, the Z axis is directed towards the north galactic pole with increasing values. One can derive the Galactic rest frame coordinates from the galactic coordinates with the transformation formula

$$\vec{x} = d \begin{pmatrix} \cos b \cos l \\ \cos b \sin l \\ \sin b \end{pmatrix} = \begin{pmatrix} X \\ Y \\ Z \end{pmatrix} \quad (2.6)$$

with  $d$  being the heliocentric distance.

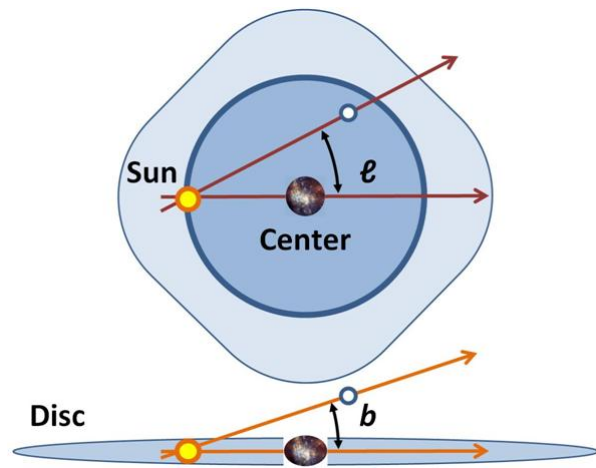


Figure 2.2: schematic drawing of the galactic coordinate system

## 2.3 Structure of the Milky Way

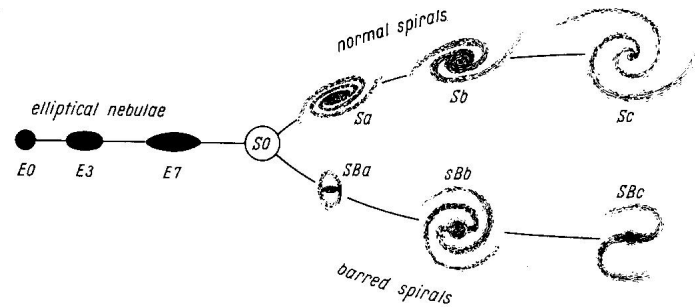


Figure 2.3: Classification of galaxies

Our Milky Way can be classified as a barred spiral galaxy (see Figure 2.3) consisting of four main parts: central bulge, bar, disk and stellar as well as dark halo.

**The central bulge** is spherical symmetric and surrounds the supermassive black hole at the center of our galaxy. It inhabits mostly relative old stars in the outer part of the bulge while massive and luminous stars can be found in the complex central region.

**The disk** encloses the galactic bulge and can be further separated into the thin disk and the thick disk. The main part of the younger stars can be found in the thin disk since star formation can happen almost only in the spiral arms of the galaxy. Older stars are more likely to be found in the thick disk.

**The stellar halo** embeds galactic bulge and disk. Its radius is yet to be determined but possibly ranges from 50 to 100kpc. It houses the oldest known stars, some in globular clusters, i.e. stable, spherical arrangements of several thousand stars.

**The dark halo** consists of dark matter and has a much larger mass than the stellar halo. Model potentials of the halo are therefore based on the distribution of the dark matter and the stellar halo is neglected.

### 2.3.1 The Galactic potential

In order to decide whether or not a star is bound to the galaxy, it is necessary to know the Galactic potential. According to Allen and Santillan [2], the potential is split up into three distinct components.

For the galactic bulge a spherically symmetric potential yields good results for objects on highly eccentric orbits but is not capable of modeling the dynamics of the innermost part of the bulge. Nevertheless it is far better than assuming a pointlike mass distribution.

It is given as

$$\Phi_{\text{Bulge}}(\rho, z) = -\frac{M_1}{(\rho^2 + z^2 + b_1)^{\frac{1}{2}}} \quad (2.7)$$

and corresponds to a total mass of  $1.41 \cdot 10^{10} M_{\odot}$ .

For the disk component a potential of the form

$$\Phi_{\text{Disk}}(\rho, z) = -\frac{M_2}{\left\{ \rho^2 + \left[ a_2 + (z^2 + b_1^2)^{1/2} \right]^{1/2} \right\}^{1/2}} \quad (2.8)$$

has been derived. The disk's total mass is  $8.56 \cdot 10^{10} M_{\odot}$ .

Finally, the potential of the halo component reads

$$\Phi_{\text{Dark matter halo}}(R) = -\left( \frac{M_3 \left( \frac{R}{a_3} \right)^{2.02}}{\left( 1 + \left( \frac{R}{a_3} \right)^{1.02} \right) R} \right) - \left( \frac{M_3}{1.02 a_3} \right) \left[ \ln \left( 1 + \left( \frac{R}{a_3} \right) \right)^{1.02} - \frac{1.02}{1 + \left( \frac{R}{a_3} \right)^{1.02}} \right]_R^{200} \quad (2.9)$$

The overall Galactic potential is the superposition of the different components:

$$\Phi_{\text{Galactic}} = \Phi_{\text{Bulge}} + \Phi_{\text{Disk}} + \Phi_{\text{Dark matter halo}} \quad (2.10)$$

In this work we use the updated constants from Irrgang et al. [11] rather than the original values from Allen and Santillan. They are listed in Table 1.

Central mass constants	$M_1 = 410.0$
	$b_1 = 0.23$
Disk constants	$M_2 = 2856.0$
	$a_2 = 4.22$
	$b_2 = 0.292$
Dark matter halo constants	$M_3 = 1018.0$
	$a_3 = 2.562$

Table 1: Constants for the Galactic potential. The mass constants are given in Galactic mass units, the lengths in kpc.

The local escape velocity determines the velocity needed for an object to overcome the gravitational forces acting on it. In the case of a star this is the velocity at which it can escape its galaxy and become unbound. Calculating the local escape velocity is a straightforward task. In order to escape the gravitational force a body's kinetic energy must exceed its potential energy at its location.

$$v_{esc} = \sqrt{\frac{2E_{pot}}{m}} \quad (2.11)$$

## 2.4 Stellar evolution

Star formation almost solely takes place in regions of relatively high molecular density called interstellar clouds. When the cloud's hydrostatic equilibrium is distorted, either by interstellar compression waves, pressure waves of supernova explosions or radiation pressure of nearby stars, it collapses. Stars mainly form in clusters since interstellar clouds are far too big and heavy to form a single star. The released gravitational energy heats the contracting matter until the conditions for hydrogen burning in the core are fulfilled.

An important tool for stellar classification is the Hertzsprung-Russell-Diagram (short: HRD, see Figure 2.4 for an example). It plots the stars' luminosity or absolute magnitude over the effective temperature or spectral type.

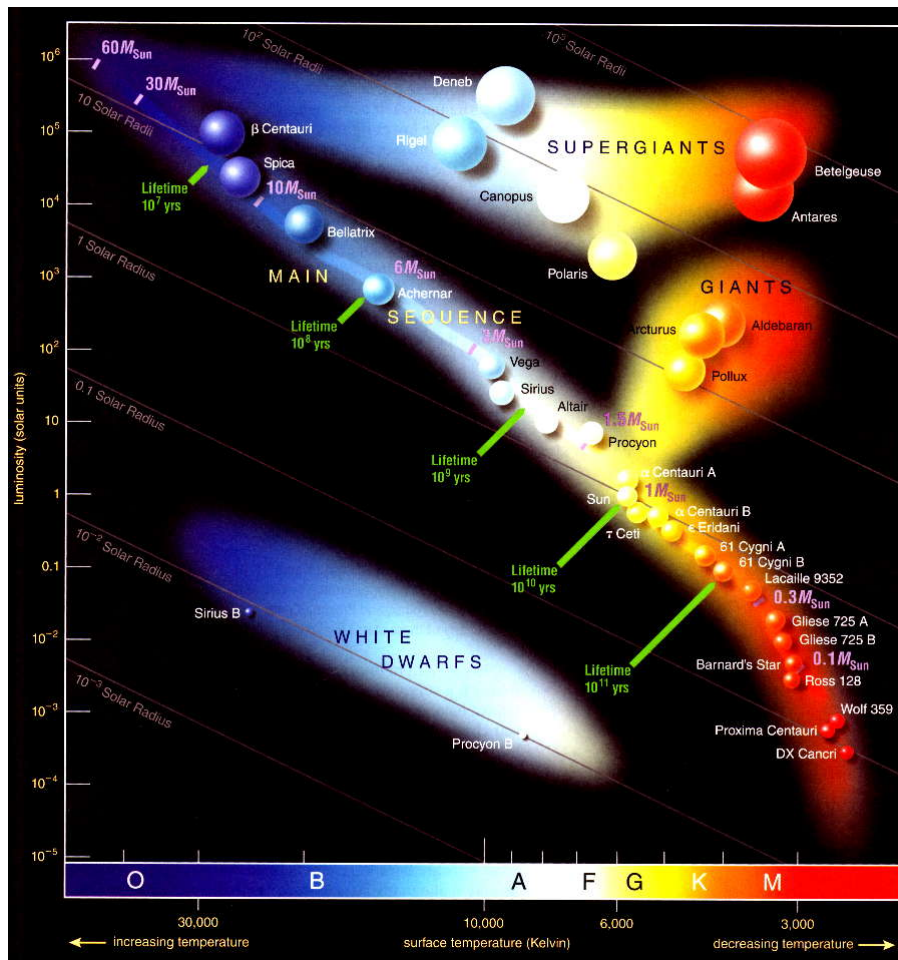


Figure 2.4: Hertzsprung-Russell-Diagram

In general, the luminosity increases to the top and the temperature decreases to the right. Thus, from a star's position in the HRD its radius can be determined. If a star is at the same effective temperature less luminous than another its radius has to be smaller and vice versa.

By far the densest population can be found for the main sequence reaching from the upper left to the lower right corner. Members of the main sequence are called dwarf stars. They are burning hydrogen at their cores and find themselves to be in hydrostatic equilibrium, i. e. the outward thermal pressure is balanced by the inward gravitational pressure. A dwarf star's position is primarily determined by its mass and chemical composition. The more massive a star, the shorter its lifetime. As soon as the hydrogen in the core is exhausted, the star evolves either to a red giant or a white dwarf, depending on its mass. Stars with a mass less than approximately 0.5 solar masses will directly become white dwarfs[1], which have no internal source of energy and cool down until they become a cool black dwarf. Other stars with masses ranging from approximately 0.5 to 8 solar masses expand to red giants. Red giants are stars that are no longer burning hydrogen in the core. If the star's mass is lower than  $2.5M_{\odot}$ , the electron gas in the core is in a degenerate state in which the pressure is no longer dependent of the temperature. Since the supply of energy can no longer be compensated by the expansion of the core, the fusion of helium to carbon begins almost immediately. The star reaches the horizontal branch on which it remains as long as hydrogen is burned in the core. Afterwards it expands and the fusion of helium takes place in a shell around the contracting core. When the helium is exhausted the star evolves to a white dwarf.

For stars with higher masses the fusion of helium is in hydrostatic equilibrium. If the mass loss, which can be very high on the asymptotic giant branch, is neglected, a star with a mass higher than  $8M_{\odot}$  collapses in a supernova, leaving behind a neutron star or a black hole. 97% of the red giants will end up as white dwarfs.[8].

### 3 Quantitative Spectroscopy

The major part of information we can get about a star is accessible over its optical spectrum. Even though we are primarily interested in the stars position and velocity, we need to figure out its atmospheric parameters. We are solving this task by setting up a model atmosphere and finding the set of parameters which gives the best fit of the synthetic spectra to the measured data.

#### 3.1 Model atmospheres

Modeling an atmosphere is a nontrivial task. Every simplification that can be made without leading to significant errors is a great advantage. When calculating the model atmosphere the following assumptions are made: since the thickness of the stellar atmosphere (the part of a star in which emission and absorption of photons takes place and thus the part we can see) is small compared to the star's radius, its geometry can be seen as plane parallel. Furthermore, we assume the local thermodynamical equilibrium. That is to say the stellar atmosphere is thought to be separated into distinct parallel layers

being homogeneous each, i.e. there are no variations perpendicular to their normal. Additionally it is seen as constant in time and as being in hydrostatic as well as in radiative equilibrium.

We now need to specify the atmospheric parameters which influence the spectrum. First of all, the effective surface temperature  $T_{\text{eff}}$  tells us how many atoms can be found in excited states and thus determines the depth of the spectral lines. Since our spectra are dominated by the Balmer lines of hydrogen it is convenient to explain this using the Balmer lines as an example. Balmer lines are transitions from the first excited state of an atom to higher excited states. If we want to observe Balmer lines the temperature has to be high enough that a non-negligible amount of atoms can be found in the first excited state. But the intensity of the Balmer lines does not increase steadily with temperature. Instead a maximum can be found at around 9500K[5]. This is because the amount of ionized hydrogen also increases with temperature. These atoms are no longer involved in the transitions because no bound electron is left. Eventually there are hardly any neutral hydrogen atoms left and the Balmer lines are getting weaker and weaker with ever increasing  $T_{\text{eff}}$ .

Next, the surface gravity induces gravitational line broadening. A higher surface gravity leads to a higher density of the atoms. The electric field created by the surrounding ions and electrons lifts the degeneracy of the energy levels by means of the Stark effect. Due to the rapidly varying electric fields we can observe a broadening of the lines.

A further source for line broadening can be found in the star's rotational velocity  $v_{\text{rot}} \sin i$ , where  $i$  stands for the angle between the star's rotational axis and the line of sight. This effect is called Doppler broadening. The wavelength of the absorbed light is Doppler shifted in opposite directions since one side of the star is moving away from and the other towards us.

Especially for metal lines that have barely visible wings an effect called thermal broadening becomes important. Due to the Maxwell velocity distribution atoms and ions in a gas are moving at different velocities, inducing a Doppler effect that leads to a broadening of the absorption lines. Figure 3.1 demonstrates the effects of the different parameters.

Lastly the metallicity affects the ratio of hydrogen and helium lines to metal lines.

### 3.2 Deriving atmospheric parameters

Using the fitsb2 routine from Napiwotzki et al. [18] and the Munari grids [17], a synthetic spectrum is fitted to the measured one via a  $\chi^2$  minimization technique based on a simplex algorithm. The grid used has a temperature range from 5250K to 10000K and a metallicity between +0.5 and -2.5. Surface gravity can be selected in the region  $2.5 < \log g < 4.5$ . The parameters  $T_{\text{eff}}$ ,  $\log g$ ,  $\log M$ ,  $v_{\text{rot}}$  and  $v_r$  can be fitted either simultaneously or separately. A set of initial values is given to fitsb2 which interpolates between the grid points until it finds a local minimum. This solution can then be taken as a new set of starting parameters. This procedure is repeated until a satisfactory match of synthetic and measured spectra is obtained.

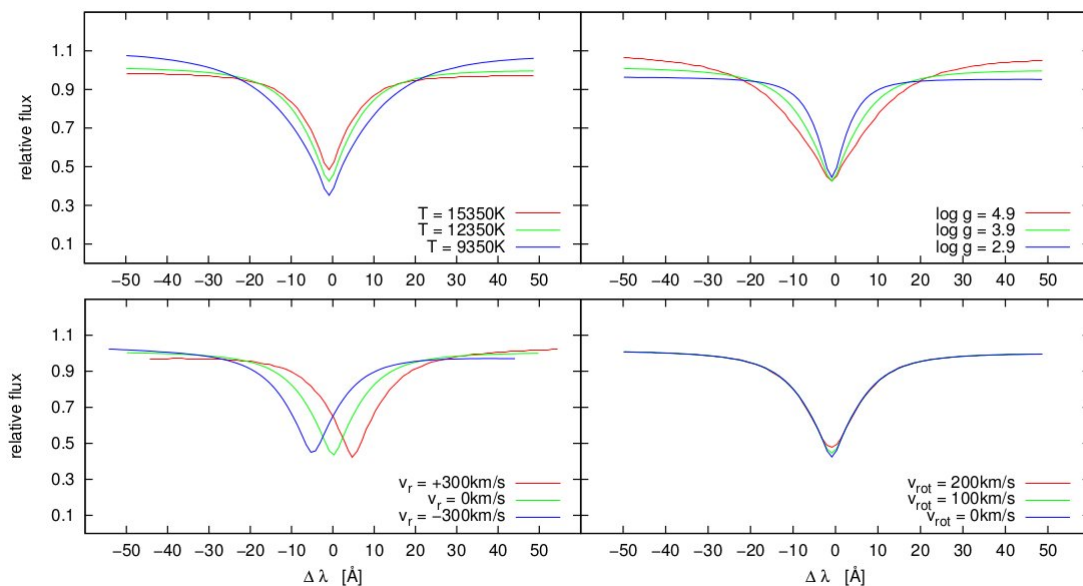


Figure 3.1: Influence of the atmospheric parameters  $T_{\text{eff}}$ ,  $\log g$ ,  $v_r$  and  $v_{\text{rot}}$ .

## 4 Kinematics

In order to get detailed knowledge about the kinematics of a star we need to calculate its position and velocity. Only with these information it is possible to say whether the star has a trajectory bound to the Galaxy or not. Additionally it can give us insight into its origin and possible formation mechanism.

The velocity is combined of the one dimensional radial velocity and the two dimensional tangential velocity. Whereas the latter is quite difficult to obtain and afflicted with rather large errors, the radial velocity is by far the easiest thing to deduce from the measured spectra. All absorption lines coming from the stellar atmosphere are Doppler shifted:

$$\frac{\Delta\lambda}{\lambda} = \frac{v_{\text{rad}}}{c} \quad (4.1)$$

Thus the radial velocity can be derived simply by comparing the wavelength of the known absorption lines with the rest wavelength once the spectral lines have been identified. In contrast, the tangential velocity is not directly accessible and requires the knowledge of the stars distance and proper motion.

### 4.1 Distance determination

Since right ascension and declination are only the projection of the star's position on the celestial sphere its distance is necessary to describe its current position.

Assuming energy conservation of the emitted light, we can state that the flux integrated over the stellar surface with radius  $R_*$  equals the flux integrated over a sphere whose

radius equals the stars distance  $d$ :

$$\oint F = 4\pi R_*^2 F = 4\pi d^2 f \quad (4.2)$$

$$\Rightarrow d = \sqrt{\frac{R_*^2 F}{f}} \quad (4.3)$$

We have to consider that we only measure the astrophysical flux  $f_V$  which is connected with the visual magnitude  $m_V$ :

$$m_V = -2.5 \log \left( f_V \frac{\text{cm}^2 \text{s} \overset{\circ}{\text{A}}}{\text{erg}} \right) - 21.107 \quad (4.4)$$

$$\Rightarrow f_V = 3.607 \cdot 10^{-9} \frac{\text{erg}}{\text{cm}^2 \text{s} \overset{\circ}{\text{A}}} \cdot 10^{-0.4m_V} \quad (4.5)$$

The visual magnitude can be calculated from the ugriz-colors provided by the SDSS with the empirical transformation formulas of Jester et al. [13]:

$$m_V = g - 0.59(g - r) - 0.01 \quad (4.6)$$

Newton's law of gravity allows us to determine the radius as we already know the surface gravity from the synthetic spectrum:

$$g = \frac{GM_*}{R_*^2} \quad (4.7)$$

$$\Rightarrow R_* = \sqrt{\frac{GM_*}{g}} \quad (4.8)$$

What is left is the astrophysical flux at the star's surface. Unfortunately it cannot simply be derived from the equation  $F = \sigma T_{\text{eff}}^4$  for a black body since we are only interested in the flux in the visual band. Furthermore  $F_V$  is influenced by the surface gravity. Putting together these equations, the distance can be calculated with the formula

$$d = 1.11 \text{kpc} \sqrt{\frac{M}{M_{\odot}} \frac{\text{cm}}{\text{gs}^2} \frac{F_V(T_{\text{eff}}, \log g)}{10^8} \frac{\text{cm}^2 \cdot \overset{\circ}{\text{A}}}{\text{erg} \cdot \text{s}}} 10^{0.4m_V} \quad (4.9)$$

But calculating the surface flux  $F_V$  requires model atmosphere, the distance calculation is therefore left to computer programs.

## 4.2 Proper motion

Proper motions describe the change in a star's coordinates which are usually given in right ascension and declination. They are therefore angular velocities measured in milliarcseconds per year. Determination of proper motions is done by comparing pictures of the star from different epochs. Distant background galaxies are assumed to remain constant in that time and are taken as reference points. The star's proper motion is then obtained via a linear fit. Knowing the distance and proper motion (with the symbol  $\mu$ ) of our star, we can derive its tangential velocity over

$$v_{\text{tan}} = \mu d = 4.74 \left( \frac{D}{1\text{pc}} \right) \left( \frac{\mu}{1''/\text{yr}} \right) \quad (4.10)$$

The prefactor arises from the unit conversion.

## 5 Analysis of J125949.16+363036.3

SDSS J125949.16+363036.3 (referred to as J1259+3630 from now on) is a very blue object and has a significant proper motion as noticed by Scholz [25]. The available data, containing coordinates, proper motion and ugriz-colors is given in Table 2.

$\alpha$	$\delta$	$\mu_\alpha$	$\mu_\delta$	
194.95486°	36.51010°	$-7.2 \pm 7.9 \frac{mas}{yr}$	$-24.3 \pm 1.7 \frac{mas}{yr}$	
u	g	r	i	z
$16.31 \pm 0.01$	$15.13 \pm 0.00$	$15.26 \pm 0.00$	$15.38 \pm 0.00$	$15.51 \pm 0.01$

Table 2: Measured data of J1259+3630

The following Section discusses the steps taken to determine the star’s nature and possible origin.

### 5.1 Modeling the atmosphere

Using the fitsb2 routine and an appropriate set of starting parameters, the atmospheric parameters  $T_{\text{eff}}$ ,  $\log g$ , and  $[Fe/H]$  were obtained. The final set of parameters is given in Table 3.

$T_{\text{eff}}$	$\log g$	$[Fe/H]$	$v_{\text{rot}}$
$8417 \pm 33\text{K}$	$4.440 \pm 0.133$	$-2.0$	$0.0 \frac{\text{km}}{\text{s}}$

Table 3: Atmospheric parameters for J1259+3630, also stating the errors given by fitsb2

Due to the limited resolution of the SDSS spectra any rotational velocity below 100km/s cannot be detected. For J1259+3630 almost every fit resulted in rotational velocities close or equal to zero. Thus for the final set of parameters it is set to zero. The remarkably low metallicity was kept fixed at  $[Fe/H] = -2.0$  because otherwise it led to surface gravities that are out of limits of the Munari grid. Those were therefore extrapolated which made the results not trustworthy. Nevertheless, the metallicity indicates that J1259+3630 is a very old halo star since younger stars generally have a higher metallicity. The metallicity of halo stars peaks around  $\log M = -1.6$  according to Prantzos [21]. The retrieved metallicity is therefore realistic, but needs to be checked nonetheless. To find an upper limit for the metallicity, the regions of possible metal lines are investigated for different metallicities (see Figure 5.1). This helps us to see at which metallicity metal lines would appear that must exceed the signal to noise ratio of the SDSS spectra. Up to a metallicity of  $[Fe/H] = -1.5$  metal lines should have been visible. Furthermore a fit focusing only on the Balmer series and the visible iron lines was made confirming the metallicity of  $[Fe/H] = -2.0$ . Last but not least this metallicity gives a slightly better overall fit

compared to the same synthetic spectrum received for the same values of  $T_{\text{eff}}$  and  $\log g$  but with a metallicity of  $[Fe/H] = -1.6$ .

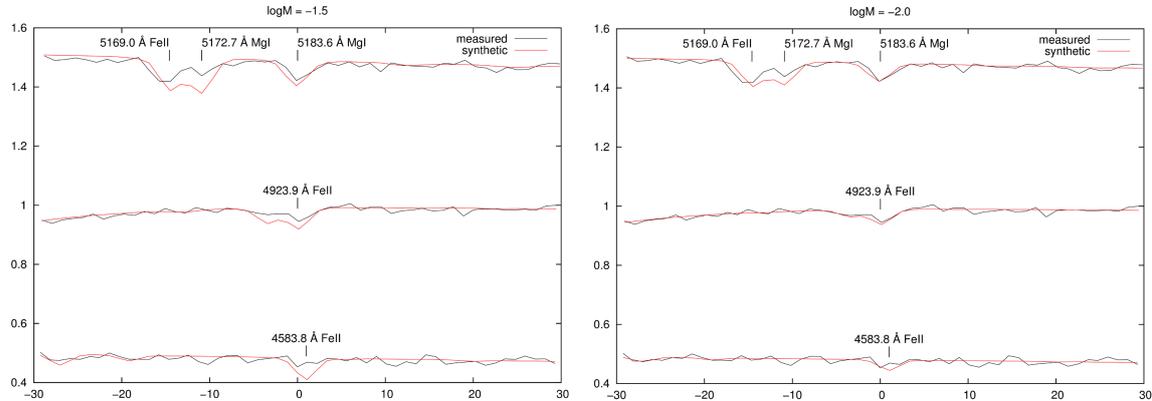


Figure 5.1: Comparing the effects of different metallicities using the example of the lines  $\lambda 4583.8 \text{ \AA}$  FeII,  $\lambda 4923.9 \text{ \AA}$  FeII,  $\lambda 5169.0 \text{ \AA}$  FeII,  $\lambda 5172.7 \text{ \AA}$  MgI and  $\lambda 5183.6 \text{ \AA}$  MgI. For metallicities higher or equal than  $[Fe/H] = -1.5$  the absorption lines would be significantly stronger than what is measured.

Another possibility to cross check the retrieved atmospheric parameters is to compare the measured color indices with the grids of synthetic colors provided by Castelli [6]. These grids contain the color indices for different combinations of  $T_{\text{eff}}$ ,  $\log g$  and  $[Fe/H]$ . As our star seems to belong to the Population II stars the grids with  $\alpha$ -enhancement were used. An interpolation between the grid points yields color indices which are consistent with the observed ones as one can see in Table 4. The difference between the values could be at least partly explained by interstellar reddening since this effect was neglected for the calculations. Finally, the CaII-line at  $\lambda 3933.66 \text{ \AA}$  is also a good evidence that J1259+3630 is a cool star. By measuring the line's Doppler shift it can be shown that it has to come at least partly from the star (see Section 5.4).

	u-g	g-r	r-i	i-z
measured	1.18	-0.13	-0.12	-0.13
synthetic	$1.029 \pm 0.024$	$-0.103 \pm 0.010$	$-0.139 \pm 0.004$	$-0.142 \pm 0.003$

Table 4: Comparison of measured and synthetic color indices

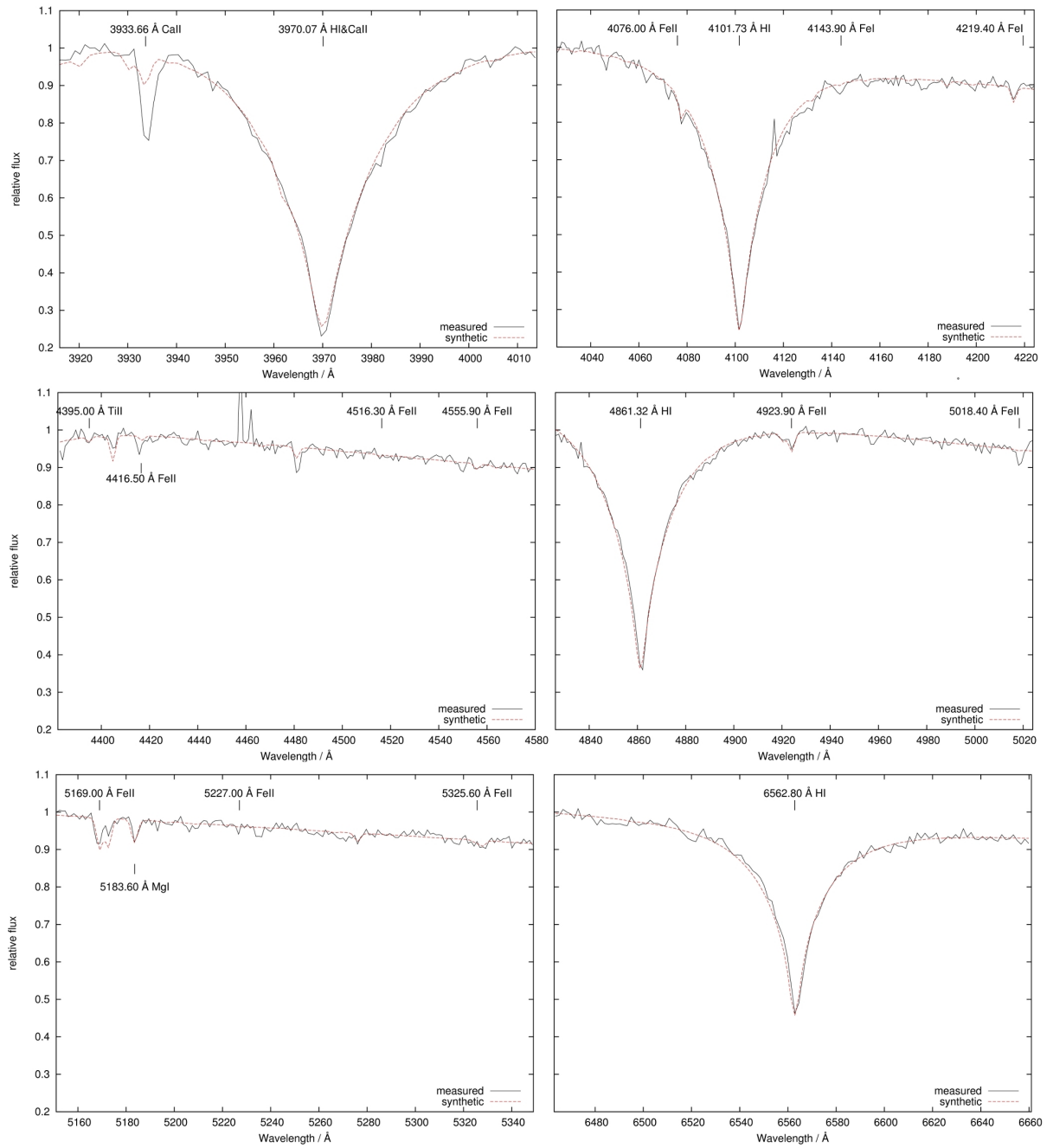


Figure 5.2: Synthetic spectrum for J1259+3630, blue part

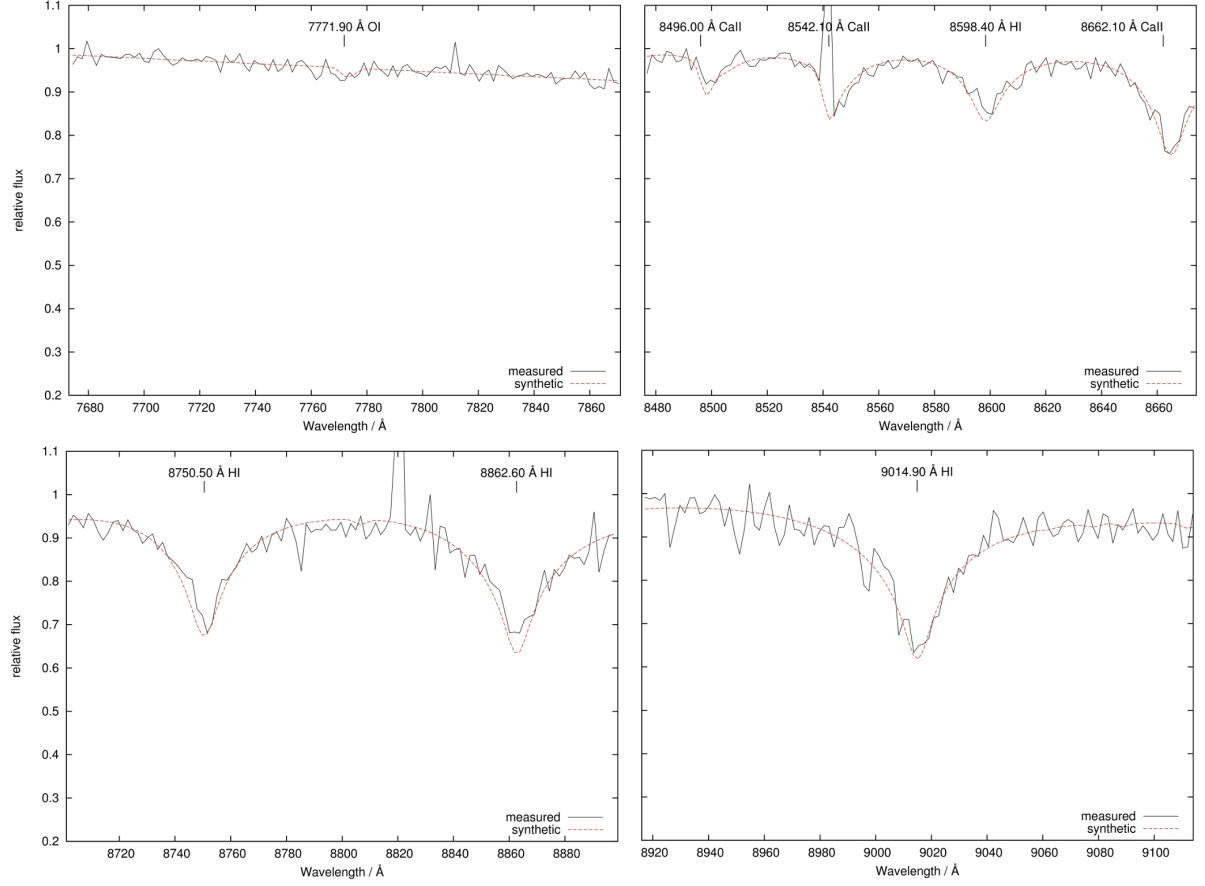


Figure 5.3: Synthetic spectrum for J1259+3630, red part

## 5.2 Mass and age determination

With the help of  $T_{\text{eff}} - \log g$ -diagrams it is possible to gain knowledge of a star's mass and age. Fortunately J1259+3630 lies well below the horizontal branch. If it layed above it we would need additional information to determine if the star belongs to the horizontal branch or to the main sequence because the evolutionary tracks of these two intersect. As for J1259+3630, we can focus on the main sequence. In this work the tracks from Schaller et al. [24] were used as well as the newer ones provided by Bertelli et al. [3]. Both tracks are given for different metal abundances  $Z$ . In this case we had to choose the tracks for  $Z=0.001$  since this is in both cases the lowest metallicity provided by the models. Note that J1259+3630 has an even lower metallicity which leads to further errors in mass. For the tracks of Schaller et al. a program written by Irrgang was available to interpolate between the evolutionary tracks for different solar masses. The Pedua tracks from Bertelli et al. lead to a slightly lower mass and about twice the age. The results are listed in Table 5, Figure 5.4 shows the star's position on the different evolutionary tracks.

All following calculations were made using the mean value and standard deviation from both tracks.

	mass	age
Schaller et al.	$1.26M_{\odot}$	1451.77Myrs
Bertelli et al.	$1.10M_{\odot}$	2855.46Myrs

Table 5: Mass and age derived from different evolutionary tracks

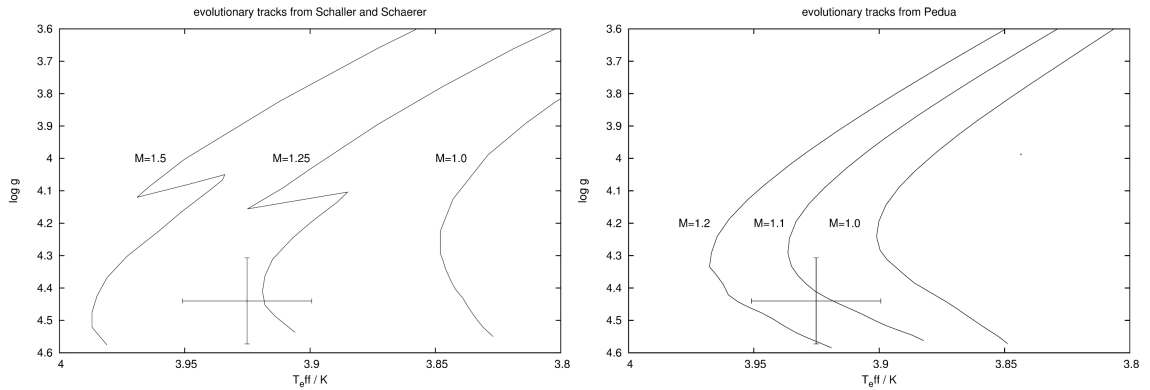


Figure 5.4:  $T_{\text{eff}} - \log g$ -diagram following Schaller et al. (left) and Bertelli et al. (right)

As stated before, the low metallicity indicates a very old Population II star. This leads to a discrepancy since the mass according to the tracks is significantly higher than the typical mass of a halo star of this age. A possible explanation for this may be that J1259+3630 is a Blue Straggler. Blue Stragglers can be easily identified in clusters. Stars of clusters are all formed at roughly the same time, meaning that their position on the HRD is solely influenced by their initial mass. As a consequence one can see a clearly defined turn off point at which the stars evolve away from the main sequence and become giants. Blue Stragglers peak out from the other cluster stars because they seem to remain on the main sequence above the turn off point. This has to mean that they are either younger than the rest or that they have gained mass during their lifetime. But as we have just said, cluster stars form at nearly the same time and thus the process of mass gaining is much more likely. The merger of two stars of a binary system[14] as well as mass transfer between two stars[15] are possible scenarios for this to happen.

Even if we could have determined the age from the evolutionary tracks the deviation would have been high. Identification of Blue Stragglers in the field is difficult because it is not possible to determine its age. Considering the metallicity J1259+3630 could easily belong to the Milky Way's oldest stars with an age up to 13.6 billion years.

### 5.3 A few words on error estimation

The program fitsb2 offers the possibility to output  $1\sigma$  errors for the fitted atmospheric parameters. The errors stated refer to the added spectrum. To check whether they are realistic or not they were compared to the mean values and standard deviations of the atmospheric parameters from the individual spectra and found to be consistent.

For later applications, where error propagation becomes increasingly difficult, a Monte Carlo simulation is used instead. This statistical approach assumes that the input parameters have a Gaussian distribution. The input parameters are varied randomly with the respective probabilities. Mean value as well as standard deviation is gained from the result's distribution.

### 5.4 Distance and velocity

As mentioned in Section 4 we use our knowledge of the absorption lines' rest wavelength to calculate the Doppler shift. To avoid possible errors from single lines all visible lines but the weakest were taken into account. For example, the  $H_\epsilon$ -line at  $\lambda 3889.05\text{\AA}$  is a blend with interstellar Calcium and could thus lead to an error for the Doppler shift. All three spectra were observed separately to check whether J1259+3630 shows variabilities in its radial velocity. SDSS spectra are typically recorded directly after one another, so it is not possible to exclude the possibility that J1259+3630 is a member of a binary system with a high period. But in the case of the individual spectra the radial velocity remains constant. Additionally, the Doppler shift of the CaII-line at  $\lambda 3933.7\text{\AA}$  was measured. Since interstellar neutral Calcium has an optical transition at the same frequency, the observed absorption line must not necessarily come from the star's atmosphere. It was found that the Doppler shift of the CaII-line matches the radial velocity obtained from the remaining lines. This is consistent with the synthetic spectra which also shows a slight amount of CaII.

For distance determination a program written by Ramspeck et al. [22] was used which is based on the formula presented in Section 4.1. Error propagation is difficult because the involved variables  $T_{\text{eff}}$ ,  $\log g$  and  $M_*$  are entangled. Instead the errors were derived from Monte Carlo statistics. With the distance now known and the proper motion the tangential velocity is calculated. The results are shown in Table 6. Note that these values are given in the celestial coordinate system and do not match the velocity in the Galactic restframe.

$d$	$v_r$	$v_{\text{tan}}$
$2849.9 \pm 525.02\text{pc}$	$-243.52 \pm 1.01 \frac{\text{km}}{\text{s}}$	$342.36 \pm 63.07 \frac{\text{km}}{\text{s}}$

Table 6: Distance and velocity of J1259+3630

## 5.5 Examination of J1259+3630's possible origin

As shown in the last section, J1259+3630's heliocentric velocity is in the order of 400km/s. But this velocity is afflicted with the relative motion of our Solar system. In order to gain comparable values for the velocity we need the Galactic rest frame velocity at the time J1259+3630 left the Galactic disk. Its ejection point was obtained tracing back its orbit by integrating backward in the Galactic potential. For this purpose an ISIS (*Integrated Spectrographic Innovative Software*) program written by Irrgang was used which uses Runge-Kutta integration methods with adaptive stepsize and offers the use of three different potentials. Firstly the potential of Allen and Santillan [2] is implemented with the updated constants from Irrgang et al. [11]. Secondly the bulge and disk potential of Miyamoto and Nagai [16] is included once with a halo component from Navarro et al. [19] and with a truncated, flat rotation curve dark matter halo from Wilkinson and Evans [27]. The program takes the stars celestial coordinates, proper motions, radial velocity and distance with the associated errors as input parameters. It traces the trajectories back in time until they reach the X-Y-plane at a predefined radius representing the Galactic disk. The stellar density outside of this region is so low that an interaction with other stars or black holes is highly unlikely. The output contains the initial and final set of parameters in galactic restframe coordinates including the time of flight, components of position and velocity vector, angular momentum and total energy. ISIS then provides convenient statistical analysis of the data.

All three potentials are taken into comparison using a Monte Carlo simulation with a depth of 50,000 for each. With 180Myrs being roughly the time of flight for all three of them, the resulting orbits were reduced by those with a time of flight greater than 500Myrs. This includes the ones that could not be traced back to the galactic disk. Additionally, the whole trajectory for the mean values of the input parameters was saved.

	Allen and Santillan	Miyamoto&Nagai/Navarro et al.
$t$	$-170.21 \pm 64.40\text{Myrs}$	$-159.61 \pm 49.01\text{Myrs}$
$r$	$5.15 \pm 5.17\text{kpc}$	$4.98 \pm 4.51\text{kpc}$
$v_{\text{mom}}$	$269.16 \pm 47.97\text{km/s}$	$269.16 \pm 47.97\text{km/s}$
$v_{\text{ejec}}$	$408.54 \pm 112.49\text{km/s}$	$409.19 \pm 106.58\text{km/s}$
$L_z$	$0.87 \pm 0.76\text{kpc}^2/\text{Myr}$	$0.88 \pm 0.78\text{kpc}^2/\text{Myr}$
Miyamoto&Nagai with rotation curve halo		
$t$	$-176.69 \pm 69.32\text{Myrs}$	
$r$	$5.28 \pm 5.48\text{kpc}$	
$v_{\text{mom}}$	$269.16 \pm 47.97\text{km/s}$	
$v_{\text{ejec}}$	$407.79 \pm 116.31\text{km/s}$	
$L_z$	$0.88 \pm 0.75\text{kpc}^2/\text{Myr}$	

Table 7: Statistics for the different potentials

First of all, one can see in Table 7 that J1259+3630's actual velocity in the Galactic restframe of  $269.16 \pm 47.99\text{km/s}$  is not particularly high. The high heliocentric veloc-

ity arises from the very steep orbits. This also indicates that J1259+3630 might have originated from a colliding satellite galaxy. With the use of a U-V-diagram as shown in Figure 5.5 J1259+3630’s affiliation to the halo population, which was already expected from the low metallicity, can be shown.

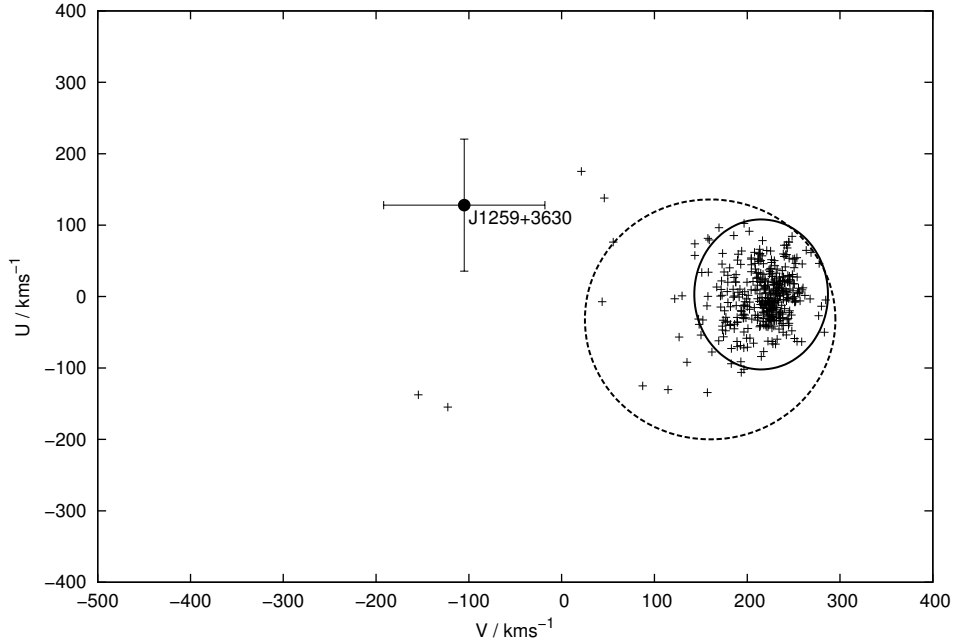


Figure 5.5: U-V diagram with a sample of white dwarfs from Pauli et al. [20] as reference. The continuous line marks the  $3\sigma$  range from the thin disk, the dashed line represents the thick disk. Being clearly outside these regions, J1259+3630 belongs to the halo population.

The different models show a very good agreement in the resulting final values (see Table 7 for details). It turns out that not a single unbound orbit can be found in any of the used potentials. Our preferred definition describes Hypervelocity stars as objects with trajectories that are not bound to the Galaxy. In this sense J1259+3630 is not a Hypervelocity star as long as the model potentials do not overestimate the total mass of the Galaxy. Brown et al. [4] focus on the star’s origin when defining Hypervelocity stars. Since the Hill’s mechanism could indeed apply to J1259+3630, it can be seen as a bound Hypervelocity star.

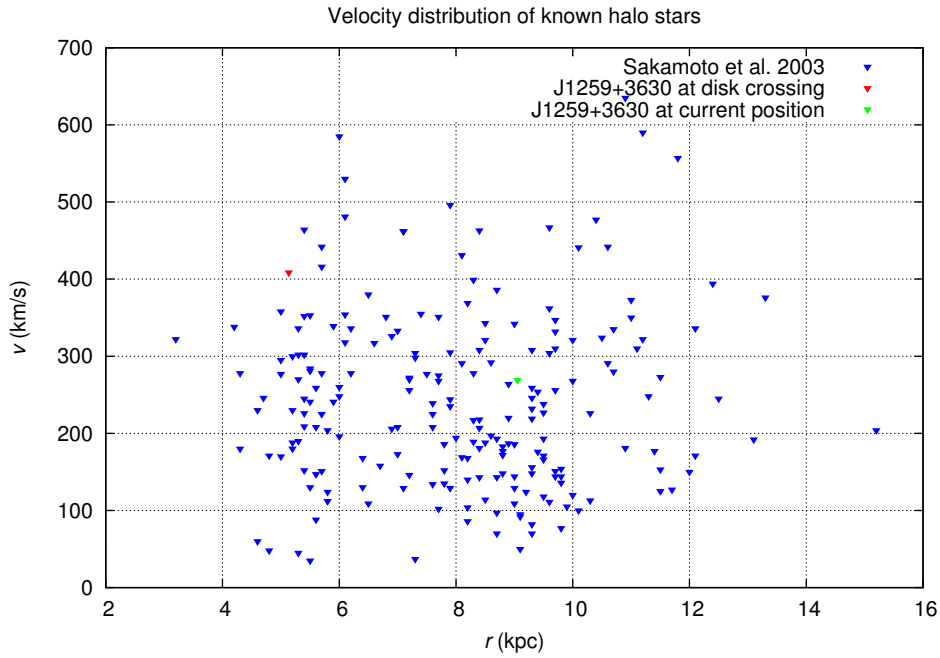


Figure 5.6: Comparison of J1259+3630’s velocity with the sample of Sakamoto et al. [23].

Figure 5.6 compares J1259+3630’s velocity and distance to the Galactic center to other halo stars recorded by Sakamoto et al. [23]. Despite the moderate current velocity, J1259+3630’s velocity exceeds the average velocity when crossing the Galactic disk. With a median distance to the Galactic center of approximately 3.6kpc about 6% of the orbits pass it within a radius of 1kpc. Further details can be seen in Figures 5.7 to 5.9. The first diagram always shows the distribution of the star’s velocity at the time it crossed the Galactic disk. In the second diagram the distance to the Galactic center at this time can be seen. The ejection velocity lies at around 400km/s for all of the model potentials. Moreover, as stated above the Hill’s mechanism could serve as an explanation for these unusual high ejection velocities since non-negligible amounts of trajectories are crossing the Galactic center within a radius of 1kpc or less.

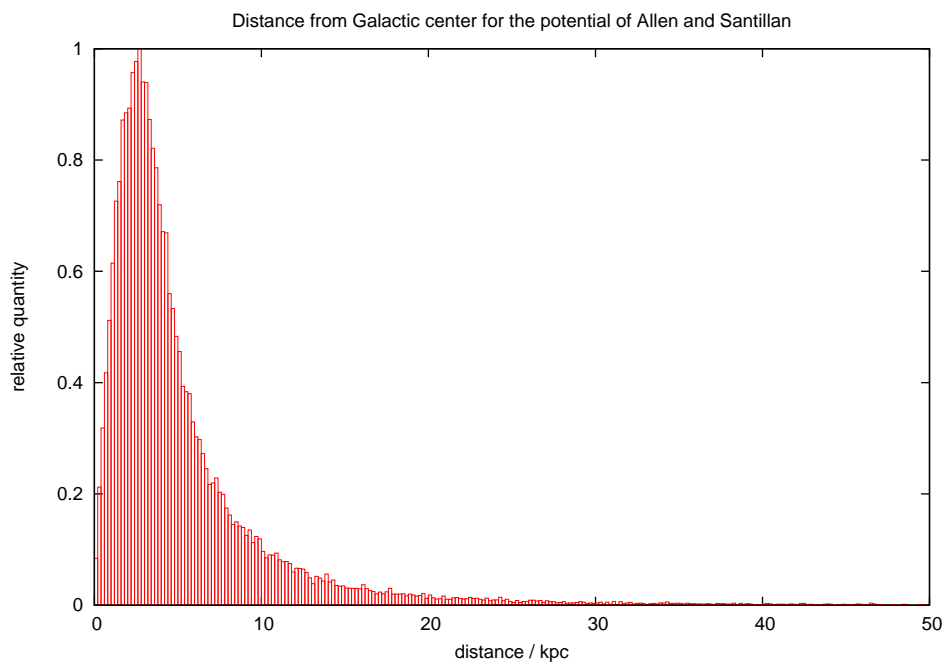
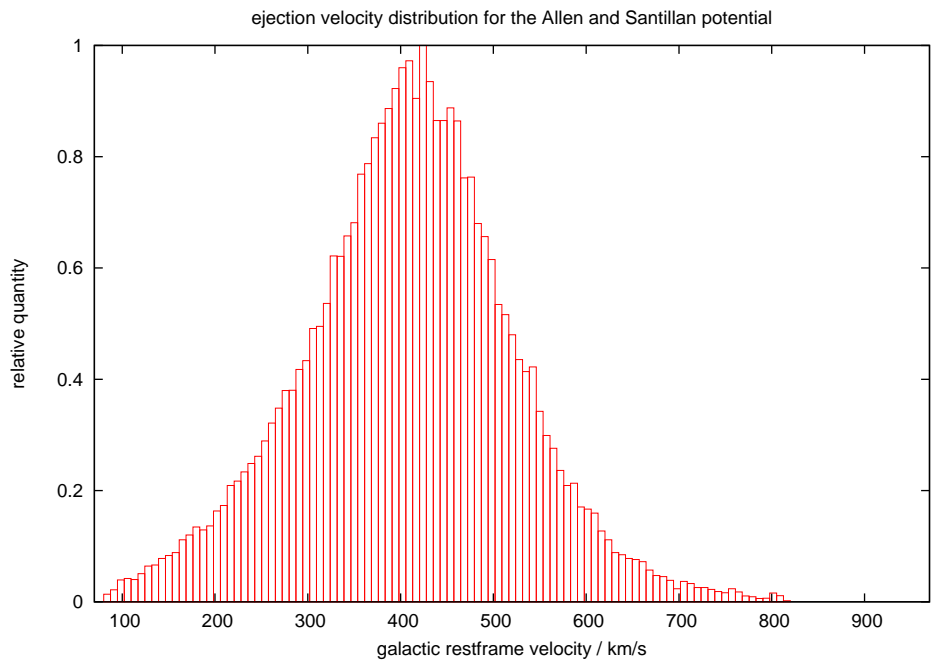


Figure 5.7: Distribution of velocity and distance to the Galactic center for the potential of Allen and Santillan with updated constants

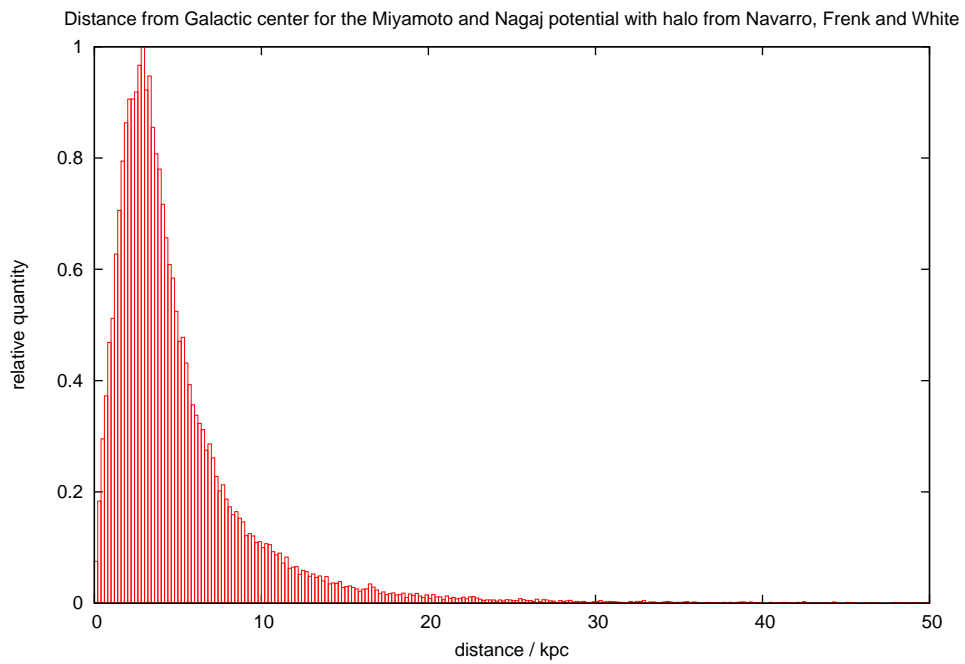
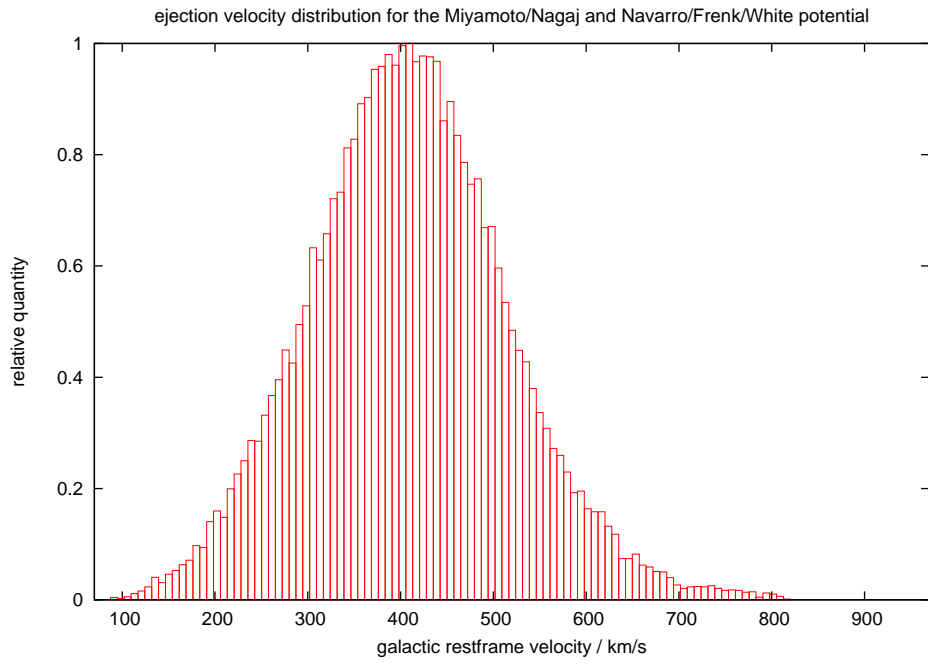


Figure 5.8: Distribution of velocity and distance to the Galactic center for the potential of Miyamoto and Nagaj with halo potential from Navarro, Frenk and White

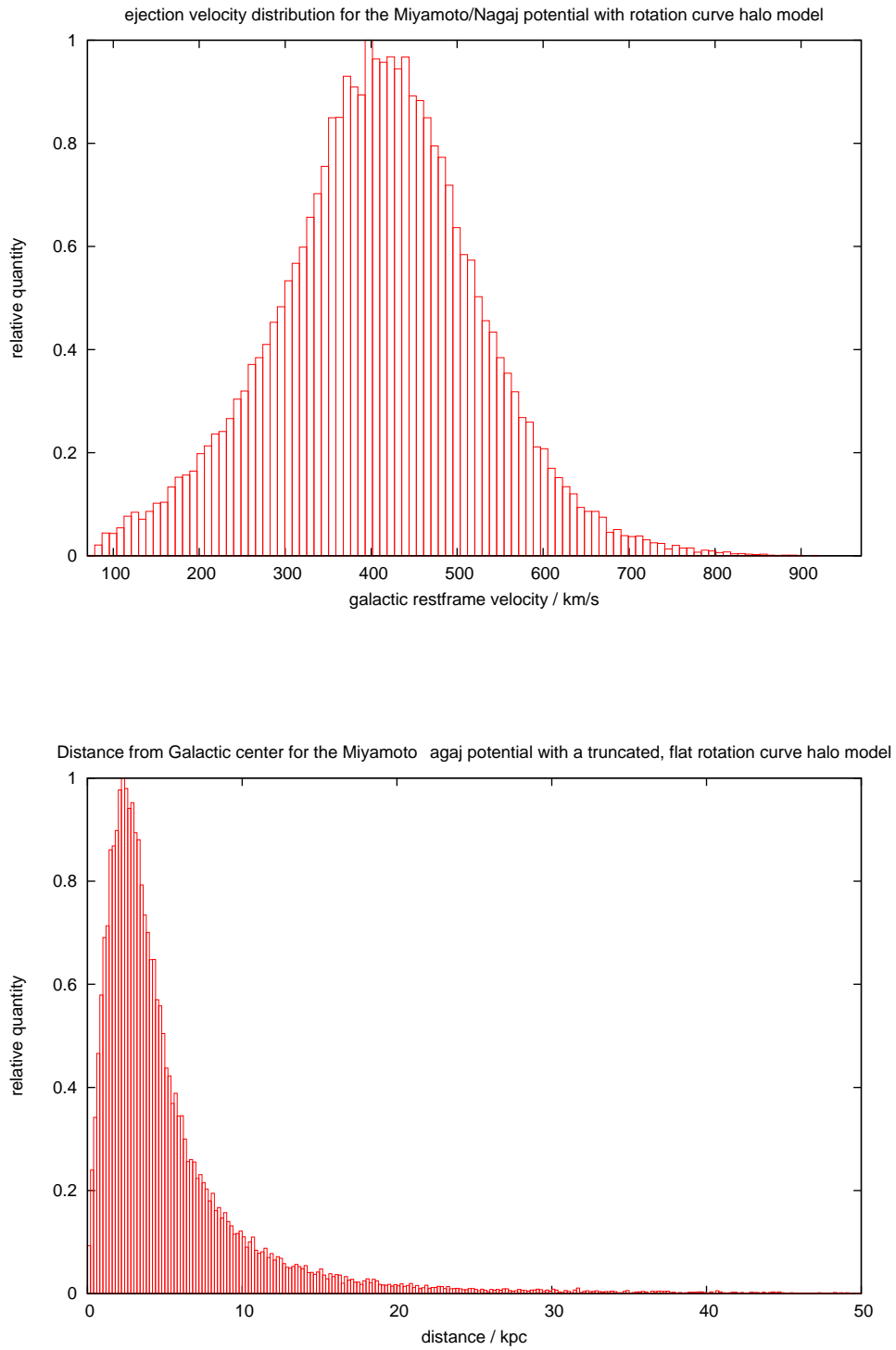


Figure 5.9: Distribution of velocity and distance to the Galactic center for the potential of Miyamoto and Nagaj with truncated, flat rotation curve dark matter halo

Figures 5.10 to 5.12 show the ejection points from the galactic disk as seen in the X-Y-plane. The errorbars state the  $1\sigma$  errors for the X and Y coordinate. Again one can see that J1259+3630 could have undergone the Hill's mechanism.

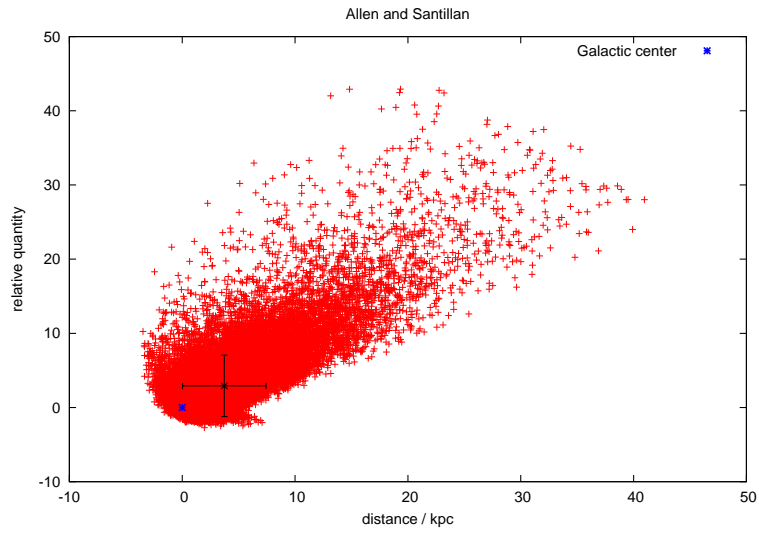


Figure 5.10: Ejection points from the Galactic disk for the Allen and Santillan potential

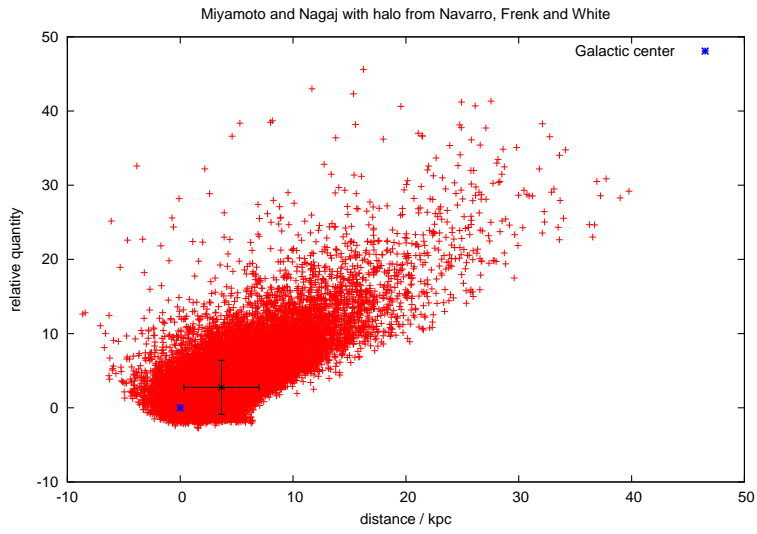


Figure 5.11: Ejection points from the Galactic disk for the Miyamoto and Nagaj potential with halo from Navarro et al.

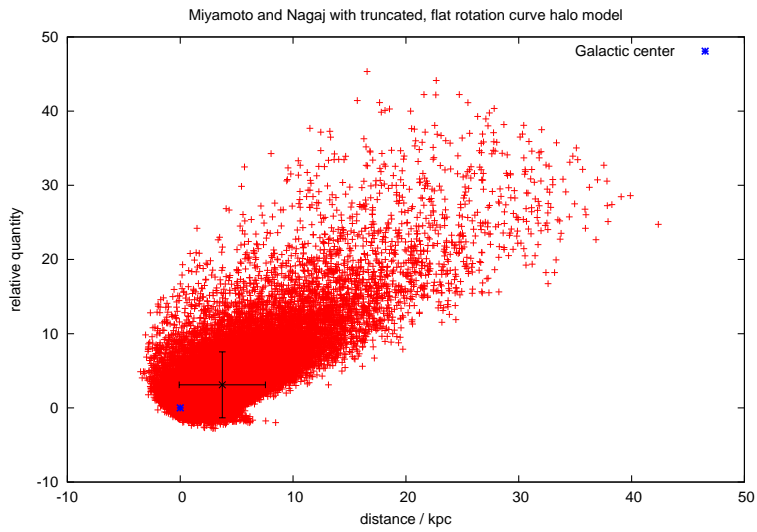


Figure 5.12: Ejection points from the Galactic disk for the Miyamoto and Nagaj potential with truncated, flat rotation curve dark matter halo

Figures 5.13 and 5.14 show the projection of J1259+3630's orbit onto the X-Y and Y-Z plane for the mean values of the input parameters in the potential of Allen and Santillan.

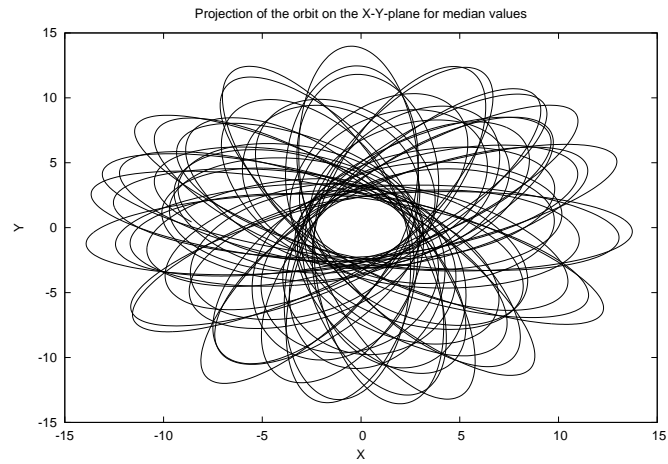


Figure 5.13: Projection of the trajectory onto the X-Y plane

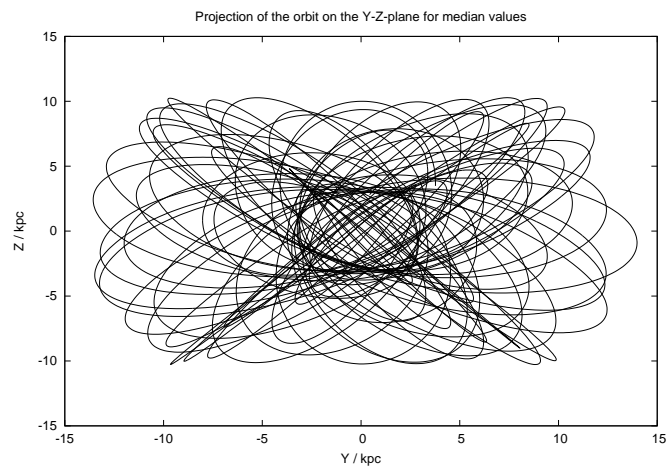


Figure 5.14: Projection of the trajectory onto the Y-Z plane

Even though the orbit is not closed it shows a periodic behavior. As one can see in Figure 5.15, J1259+3630 frequently reaches near the Galactic center and then leaves again.

If there has been an interaction with the supermassive black hole, it could have been anytime in the past. These calculations have to be taken with caution nevertheless. The used potentials are based on mass distributions and therefore do not model the disturbance of nearby stars that would rather correspond to pointlike masses. This fact becomes even more important in the dense stellar regions of the bulge. Every crossing of the galactic disk would presumably lead to a small change in the star's direction, meaning that in reality J1259+3630's trajectory most likely may not be periodic at all.

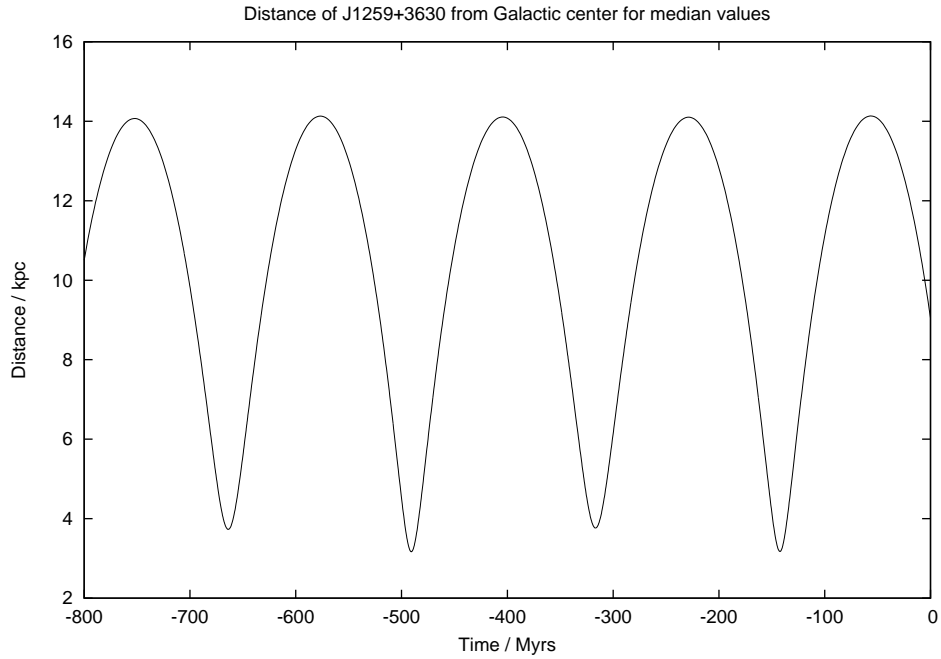


Figure 5.15: J1259+3630's distance to the Galactic center over time

## 6 Summary and Outlook

In the course of this work the star J125949.16+363036.3 with a high proper motion was examined. Based on SDSS spectra the atmospheric parameters, mass, age, distance and radial velocity were determined. A Monte Carlo simulation of the star's trajectories gave insight to its possible origin. Even though J125949.16+363036.3 does not belong to the class of unbound Hypervelocity Stars it remains an interesting object for further observations as its very low metallicity and relatively high mass indicate that it is a Blue Straggler. In general, stars with high velocities that have also bound orbits can be used to calculate a lower limit for the mass of the Milky Way. But in the case of J1259+3630 the Galactic rest frame velocity is not particularly high. Furthermore, the orbit calculation is influenced by the large errors of the proper motions, leading to a wide spread of possible crossing points of the Galactic disk. With the data from the GAIA (*Global Astrometric Interferometer for Astrophysics*) mission, starting in autumn 2013, more accurate proper motions will be obtainable.

## List of Figures

2.1	Equatorial coordinate system. Source: <a href="http://star-www.st-and.ac.uk/~fv/webnotes/RADEC.GIF">http://star-www.st-and.ac.uk/~fv/webnotes/RADEC.GIF</a> . . . . .	5
2.2	Galactic coordinate system. Source: <a href="http://en.wikipedia.org/wiki/File:Galactic_coordinates.JPG">http://en.wikipedia.org/wiki/File:Galactic_coordinates.JPG</a> . . . . .	6
2.3	Classification of galaxies. Source: <a href="http://ned.ipac.caltech.edu/level5/Sandage/Figures/Figure2.jpeg">http://ned.ipac.caltech.edu/level5/Sandage/Figures/Figure2.jpeg</a> . . . . .	7
2.4	Hertzsprung-Russell-Diagram. Source: <a href="http://deskarati.com/wp-content/uploads/2012/03/Hertzsprung-Russell-Diagram">http://deskarati.com/wp-content/uploads/2012/03/Hertzsprung-Russell-Diagram</a> . . . . .	9
3.1	Influence of the atmospheric parameters. Source: Ziegerer [29] . . . . .	12
5.1	Comparison of different metallicities . . . . .	16
5.2	Synthetic spectrum for J1259+3630, blue part . . . . .	17
5.3	Synthetic spectrum for J1259+3630, red part . . . . .	18
5.4	$T_{\text{eff}} - \log g$ -diagram . . . . .	19
5.5	U-V diagram . . . . .	22
5.6	Comparison of J1259+3630's velocity with the sample of Sakamoto et al. [23]. . . . .	23
5.7	Distribution of velocity and distance to the Galactic center for the potential of Allen and Santillan with updated constants . . . . .	24
5.8	Distribution of velocity and distance to the Galactic center for the potential of Miyamoto and Nagaj with halo potential from Navarro, Frenk and White . . . . .	25
5.9	Distribution of velocity and distance to the Galactic center for the potential of Miyamoto and Nagaj with truncated, flat rotation curve dark matter halo . . . . .	26
5.10	Ejection points from the Galactic disk for the Allen and Santillan potential . . . . .	27
5.11	Ejection points from the Galactic disk for the Miyamoto and Nagaj potential with halo from Navarro et al. . . . .	28
5.12	Ejection points from the Galactic disk for the Miyamoto and Nagaj potential with truncated, flat rotation curve dark matter halo . . . . .	28
5.13	Projection of the trajectory onto the X-Y plane . . . . .	29
5.14	Projection of the trajectory onto the Y-Z plane . . . . .	29
5.15	J1259+3630's distance to the Galactic center over time . . . . .	30

## List of Tables

1	Constants for the Galactic potential . . . . .	8
2	Measured data of J1259+3630. Source: <a href="http://skyserver.sdss3.org/dr9/en/tools/quicklook/quickobj.asp?id=1237664818217943078">http://skyserver.sdss3.org/dr9/en/tools/quicklook/quickobj.asp?id=1237664818217943078</a> , . . . . .	15
3	Atmospheric parameters for J1259+3630 . . . . .	15

4	Comparison of measured and synthetic color indices . . . . .	16
5	Mass and age derived from different evolutionary tracks . . . . .	19
6	Distance and velocity of J1259+3630 . . . . .	20
7	Statistics for the different potentials . . . . .	21

## References

- [1] F. C. Adams and G. Laughlin. A dying universe: the long-term fate and evolution of astrophysical objects. *Reviews of Modern Physics*, 69:337–372, April 1997. doi: 10.1103/RevModPhys.69.337.
- [2] C. Allen and A. Santillan. An improved model of the galactic mass distribution for orbit computations. *Revista Mexicana de Astronomia y Astrofisica*, 22:255–263, October 1991.
- [3] G. Bertelli, L. Girardi, P. Marigo, and E. Nasi. Scaled solar tracks and isochrones in a large region of the Z-Y plane. I. From the ZAMS to the TP-AGB end for 0.15-2.5  $M_{sun}$  stars. *Astronomy and Astrophysics*, 484:815–830, June 2008. doi: 10.1051/0004-6361:20079165.
- [4] W. R. Brown, M. J. Geller, S. J. Kenyon, and M. J. Kurtz. Discovery of an Unbound Hypervelocity Star in the Milky Way Halo. *Astrophysical Journal, Letters*, 622:L33–L36, March 2005. doi: 10.1086/429378.
- [5] B. W. Carroll and D. A. Ostlie. *An introduction to modern astrophysics and cosmology*. July 2006.
- [6] Castelli. Grids of sloan indices from odnew atlas9 models. URL <http://wwwuser.oat.ts.astro.it/castelli/colors/sloan.html>.
- [7] H. Edelmann, R. Napiwotzki, U. Heber, N. Christlieb, and D. Reimers. HE 0437-5439: An Unbound Hypervelocity Main-Sequence B-Type Star. *Astrophysical Journal, Letters*, 634:L181–L184, December 2005. doi: 10.1086/498940.
- [8] G. Fontaine, P. Brassard, and P. Bergeron. The Potential of White Dwarf Cosmochronology. *Publications of the ASP*, 113:409–435, April 2001. doi: 10.1086/319535.
- [9] J. G. Hills. Hyper-velocity and tidal stars from binaries disrupted by a massive Galactic black hole. *Nature*, 331:687–689, February 1988. doi: 10.1038/331687a0.
- [10] H. A. Hirsch, U. Heber, S. J. O’Toole, and F. Bresolin. US 708 - an unbound hyper-velocity subluminal O star. *Astronomy and Astrophysics*, 444:L61–L64, December 2005. doi: 10.1051/0004-6361:200500212.
- [11] A. Irrgang, B. Wilcox, E. Tucker, and L. Schiefelbein. Milky Way mass models for orbit calculations. *Astronomy and Astrophysics*, 549:A137, January 2013. doi: 10.1051/0004-6361/201220540.
- [12] Andreas Irrgang. Spectroscopy of the runaway b-star hip 60350. Diplomarbeit, Friedrich-Alexander-Universitaet Erlangen-Naernberg, November 2009.

- [13] S. Jester, D. P. Schneider, G. T. Richards, R. F. Green, M. Schmidt, P. B. Hall, M. A. Strauss, D. E. Vanden Berk, C. Stoughton, J. E. Gunn, J. Brinkmann, S. M. Kent, J. A. Smith, D. L. Tucker, and B. Yanny. The Sloan Digital Sky Survey View of the Palomar-Green Bright Quasar Survey. *Astronomical Journal*, 130:873–895, September 2005. doi: 10.1086/432466.
- [14] N. Leigh, A. Sills, and C. Knigge. An analytic model for blue straggler formation in globular clusters. *Monthly Notices of the RAS*, 416:1410–1418, September 2011. doi: 10.1111/j.1365-2966.2011.19136.x.
- [15] P. Lu, L. C. Deng, and X. B. Zhang. Blue straggler formation via close binary mass transfer. *Monthly Notices of the RAS*, 409:1013–1021, December 2010. doi: 10.1111/j.1365-2966.2010.17356.x.
- [16] M. Miyamoto and R. Nagai. Three-dimensional models for the distribution of mass in galaxies. *Publications of the ASJ*, 27:533–543, 1975.
- [17] U. Munari, R. Sordo, F. Castelli, and T. Zwitter. An extensive library of 2500 to 10500 Å synthetic spectra. *Astronomy and Astrophysics*, 442:1127–1134, November 2005. doi: 10.1051/0004-6361:20042490.
- [18] R. Napiwotzki, C. Karl, G. Nelemans, L. Yungelson, N. Christlieb, H. Drechsel, U. Heber, D. Homeier, B. Leibundgut, D. Koester, T. R. Marsh, S. Moehler, E.-M. Pauli, D. Reimers, and A. Renzini. Close binary white dwarfs and supernovae Ia. In G. Tovmassian and E. Sion, editors, *Revista Mexicana de Astronomia y Astrofisica Conference Series*, volume 20 of *Revista Mexicana de Astronomia y Astrofisica Conference Series*, pages 113–116, July 2004.
- [19] J. F. Navarro, C. S. Frenk, and S. D. M. White. A Universal Density Profile from Hierarchical Clustering. *Astrophysical Journal*, 490:493, December 1997. doi: 10.1086/304888.
- [20] E.-M. Pauli, R. Napiwotzki, U. Heber, M. Altmann, and M. Odenkirchen. 3D kinematics of white dwarfs from the SPY project. II. *Astronomy and Astrophysics*, 447:173–184, February 2006. doi: 10.1051/0004-6361:20052730.
- [21] N. Prantzos. The metallicity distribution of the halo and the satellites of the Milky Way in the hierarchical merging paradigm. *Astronomy and Astrophysics*, 489:525–532, October 2008. doi: 10.1051/0004-6361:20079330.
- [22] M. Ramspeck, U. Heber, and S. Moehler. Early type stars at high galactic latitudes. I. Ten young massive B-type stars. *Astronomy and Astrophysics*, 378:907–917, November 2001. doi: 10.1051/0004-6361:20011246.
- [23] T. Sakamoto, M. Chiba, and T. C. Beers. The mass of the Milky Way: Limits from a newly assembled set of halo objects. *Astronomy and Astrophysics*, 397:899–911, January 2003. doi: 10.1051/0004-6361:20021499.

- [24] G. Schaller, D. Schaerer, G. Meynet, and A. Maeder. New grids of stellar models from 0.8 to 120 solar masses at  $Z = 0.020$  and  $Z = 0.001$ . *Astronomy and Astrophysics, Supplement*, 96:269–331, December 1992.
- [25] Dr. Ralf-Dieter Scholz. Liste moeglicher hyper-velocity sterne.
- [26] Franz Alfred Tillich. *Hyper-velocity Stars - a spectroscopic and kinematic study of blue stars*. PhD thesis, Friedrich-Alexander-Universitaet Erlangen-Nuernberg, 2010.
- [27] M. I. Wilkinson and N. W. Evans. The present and future mass of the Milky Way halo. *Monthly Notices of the RAS*, 310:645–662, December 1999. doi: 10.1046/j.1365-8711.1999.02964.x.
- [28] Q. Yu and S. Tremaine. Ejection of Hypervelocity Stars by the (Binary) Black Hole in the Galactic Center. *The Astrophysical Journal*, 599:1129–1138, December 2003. doi: 10.1086/379546.
- [29] Eva Ziegerer. Hypervelocity sterne. Diplomarbeit, Friedrich-Alexander-Universitaet Erlangen-Nuernberg, 2011.